Design, Set-Up, and First Ignition of the RF Helicon-based Plasma Thruster

SPACE PROPULSION 2020+1

Online / 17-19 March 2021

F. Romano* (1), Y.-A. Chan (1), G. Herdrich (1), C. Traub (1), S. Fasoulas (1), P. C.E. Roberts (2), N. Crisp (2), B. E.A. Holmes (2), S. Edmondson (2), S. Haigh (2), S. Livadiotti (2), A. Macario-Rojes (2), V.T. A. Oiko (2), L.A. Sinpetru (2), K. Smith (2), J. Becedas (3), V. Sulliotti-Linner (3), M. Bisgaard (4), S. Christensen (4), V. Hanessian (4), T. Kauffman Jensen (4), J. Nielsen (4), D. Garcia-Almiñana (5), M. Garcia-Berenguer (5), S. Rodriguez-Donaire (5), M. Sureda (5), D. Kataria (6), B. Belkouchi (7), A. Conte (7), S. Seminari (7)

*(1) Institute of Space Systems (IRS), University of Stuttgart, Pfaffenwaldring 29, 70569, Stuttgart, Germany, *romano@irs.uni-stuttgart.de*

(2) The University of Manchester, Oxford Road, Manchester, M13 9PL, UK.

(3) Elecnor Deimos Satellite Systems, C/ Francia 9, 13500, Puertollano, Spain

(4) GomSpace AS, Langagervej 6, Aalborg East 9220, Denmark

(5) UPC-BarcelonaTECH, Colom 11, TR5 - 08222 Terrassa, Spain

(6) Mullard Space Science Laboratory, University College London, Holmbury St. Mary, Dorking, Surrey, RH5 6NT, UK

(7) Euroconsult, 86 Boulevard de Sébastopol, 75003 Paris, France

KEYWORDS

Atmosphere-Breathing Electric Propulsion - ABEP - VLEO - Helicon Plasma Thruster - Birdcage

ABSTRACT

To extend missions lifetime at very low orbits (VLO), an efficient propulsion system is required for drag compensation. Atmosphere-Breathing Electric Propulsion (ABEP) is a concept that collects atmospheric particles to be used as propellant for an electric thruster. The system could nullify the onboard propellant storage requirements. Moreover, it can be applied to any celestial body with atmosphere (Mars, Venus, Titan, etc.), enabling novel missions at VLO for long periods. Challenging is the operation with atmospheric propellant, especially atomic oxygen (AO), highly present in Earth orbit, that causes erosion of (not only) major propulsion system components. The RF helicon-based plasma thruster is designed, built, and set-into operation. It is contactless and features a novel antenna called the birdcage antenna, derived from heritage of magnetic resonance imaging (MRI) machines. A static magnetic field is applied as 1) required boundary condition for the helicon wave formation in the plasma, and 2) provides further electromagnetic acceleration of the plasma. The first tests on Ar, N_2, and O_2 show a low input power requirement $P_f \sim 60\,\mathrm{W}$, easy ignition, and minimized reflected power P_r. Finally, a B-dot magnetic inductive probe is designed and integrated to verify the presence of helicon waves in the plasma plume.

1 ATMOSPHERE-BREATHING ELECTRIC PROPULSION

The RF Helicon-based Plasma Thruster is designed within the H2020 DISCOVERER project [1], that aims to redesign very low Earth orbit (VLEO $< 450\,\mathrm{km}$) platforms by researching low drag materials, aerodynamic attitude control, and Atmosphere-Breathing Electric Propulsion (ABEP), see Fig. 1. Orbiting in VLEO can open a variety of novel space missions [1], however, the aerodynamic drag limits the mission's lifetime. If a propulsion system is required, the limit is then imposed by the amount of propellant that can be carried. An ABEP system, instead, collects the atmospheric particles in VLEO by an intake and feeds an electric thruster. This can counteract the drag and remove to requirement of carrying propellant on-board. Moreover, it can be applied to any planet with atmosphere. The contact-less nature of the RF helicon-based plasma thruster removes the erosion issues due to the use of AO as propellant (dominant alongside N_2 in VLEO), and produces a quasi-neutral plasma plume, removing the requirement of a neutralizer working on atmospheric

propellant as well. The thruster is based on a birdcage antenna, a device developed decades ago for magnetic resonance imaging (MRI) machines [2]. The thruster design minimizes electrical losses and produces a convenient electromagnetic field configuration for quasi-neutral plasma acceleration in combination with an applied magnetic field that also provides the boundary conditions for the formation of helicon waves. Finally, to verify their presence within the plasma discharge, a magnetic inductive B-dot probe is designed and integrated.

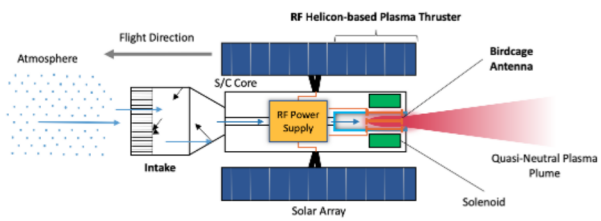

Figure 1: ABEP Concept [3].

2 RF HELICON-BASED PLASMA THRUSTER DESIGN

The requirements set within DISCOVERER are of an RF contactless plasma thruster operating on variable mixtures of N_2 and AO as propellant with $P_{in} < 5kW$. The contactless nature of the thruster is crucial to cope with the chemically aggressive AO, one of the main species in VLEO. In conventional EP systems, such as gridded ion and Hall-effect thrusters (GIT and HET), erosion of grids and discharge channels will reduce thruster's performance over time rapidly [4, 5]. Moreover, a neutralizer is not required, a device that is challenging to design for atmospheric propellant operation [6]. The first version of the thruster is a model for laboratory testing, designed for maximum (technical) flexibility to allow for easy modifications for optimization purposes. Following the design of mechanical and vacuum interfaces, the crucial element of the thruster design is the antenna and its respective tuning which will be described in the following sections.

3 RF CIRCUIT DESIGN

According to investigation using HELIC and ADAMANT [7, 3] a frequency higher than $f = 27.12\,\mathrm{MHz}$ is preferable for easier ignition (important for ABEP operation), and for better power absorption at higher plasma densities, when associated with an applied magnetic field. An RF-Generator and auto-matching network operates at $f = 40.68\,\mathrm{MHz}$ have been acquired. The thruster discharge channel is of $\phi = 37\,\mathrm{mm}$ inner diameter. As antenna and plasma are seen in the RF circuit as an equivalent impedance $\vec{Z} = \vec{R} + j\vec{X}$ [8], with both real (resistance R) and imaginary (reactance X) components, where the reactance is a in Eq. 1.

$$X = X_L + X_C = 2\pi f L + \left(-\frac{1}{2\pi f C}\right) \tag{1}$$

Finally, the whole system, including RF generator, matching network, cabling, and connectors must be optimized [9]. The power transfer from an AC source (RF generator) to its load (the thruster) is maximized only if the load's impedance Z_L is "matched" to that of the source Z_S. Industry standard is $Z_S = (50 + 0\mathrm{i})\,\Omega$ purely resistive output. The matching network dynamically creates a resonant circuit with the load, matching it to Z_S by variable capacitors and inductors. It acts as protection for the RF generator by eliminating the reflected power reaching it. As the matching network does not improve the load, an optimum design of the load is required. The thruster's antenna can be optimized, but the plasma is a variable Z that needs a further dynamic matching and tuning. Within the RF Helicon-base plasma thruster design, a novel optimized antenna, the birdcage antenna, is built and combined with a combined RF circuit optimization, see Fig. 2.

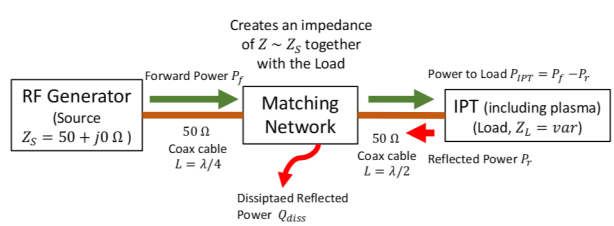

Figure 2: Thruster Optimized Circuit Schematics [3].

4 THE BIRDCAGE ANTENNA

The birdcage antenna has been developed and optimized for Magnetic Resonance Imaging (MRI) [2]. They are made of two end-rings, connected by equally spaced legs. Capacitors are placed in between the legs at the end ring, or in the middle of the legs, to tune the antenna to resonate at the desired frequency.They can be designed as low-pass, high-pass, or band-pass frequency response depending on the location of the capacitors, see Fig. 3. The high-pass configuration is selected for the thruster. If the antenna is operated at the $k = 1$ resonance mode, a homogeneous transversal magnetic field is generated, and can be either linearly or circularly polarized depending on the antenna feeding. At resonance, $X = 0\,\Omega$, therefore representing a partially matched load. By changing the relative position of RF feeding and ground, the amplitude of Z can be tuned as well [10].

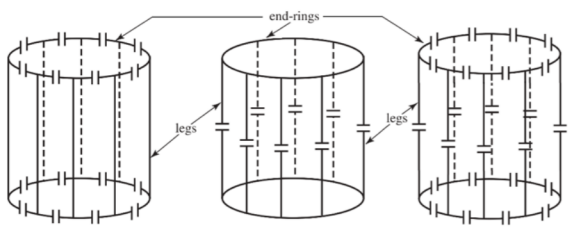

Figure 3: The Birdcage Antenna [3].

Birdcage antennae operate on the principle that a sinusoidal current distribution over a cylindrical surface induces a homogeneous transversal magnetic field within the volume itself. To calculated the required capacitance for the desired resonance frequency, the inductances of the antenna's leg L_{Leg} and end-ring L_{ER} have to be calculated. For the high pass design Eq. 2 is valid, for $k = 0, 1, ..., N/2$, where N is the number of legs..

$$\omega_{k_{HP}} = \left[C \left(L_{ER} + 2L_{Leg} \sin^2 \frac{\pi k}{N} \right) \right]^{-1/2} \tag{2}$$

In terms of electromagnetic (EM) fields, the B-field created by the birdcage, see Fig. 4, is $\vec{B}_1$ along y, the respective electric field $\vec{E}_1$ is perpendicular to $\vec{B}_1$, along x. Since $\vec{B}_1$ is linearly polarized, its direction will switch along y on each cycle, and so will $\vec{E}_1$ along x. An additional external magnetic field is provided along the z axis, $\vec{B}_0$, to provide the boundary condition for the formation of helicon waves that increase plasma discharge efficiency. The resulting EM fields can provide a drift velocity $\vec{v}_E = \vec{E} \times \vec{B}$ to both ions and electrons in the same direction z, see Eq. 3, therefore partial thrust, further enhanced by the magnetic nozzle effect provided by the applied magnetic field $\vec{B}_0$ that diverges in the exhaust region. A quasi-neutral plasma exhaust that does not require a neutralizer is produced. Such results support the use of a birdcage antenna for a contactless plasma thruster application. Currently, helicon plasmas for fusion research using birdcage antennae exist and operate at $f = 13.56\,\text{MHz}$ for RF powers up to $P = 10\,\text{kW}$ [10, 11, 12, 13, 14].

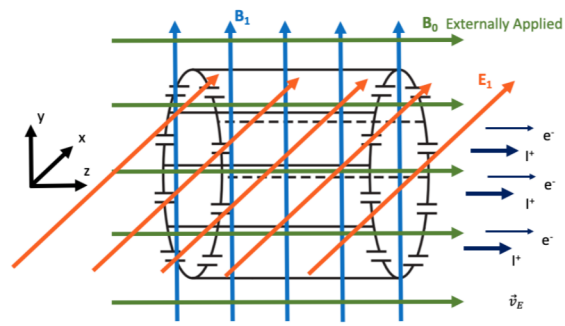

Figure 4: The Birdcage Antenna EM Fields [3].

$$\vec{v}_E = \frac{1}{\vec{B}^2} \begin{Vmatrix} \hat{x} & \hat{y} & \hat{z} \\ E_1 & 0 & 0 \\ 0 & B_1 & B_0 \end{Vmatrix} = \frac{1}{{B_0}^2 + {B_1}^2} \begin{Bmatrix} 0 \\ -E_1 B_0 \\ E_1 B_1 \end{Bmatrix} \tag{3}$$

5 RF HELICON-BASED PLASMA THRUSTER DESIGN AND VERIFICATION

The thruster is composed of the following components: propellant injector, discharge channel, birdcage antenna, Faraday shield, solenoid, and support structure, see Fig. 5.

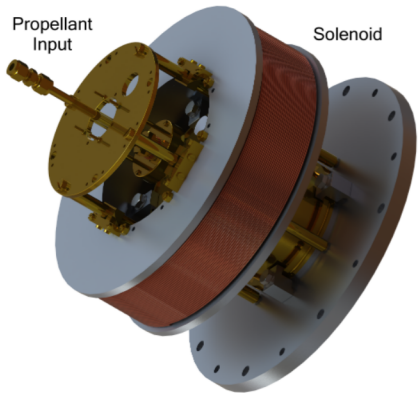

Figure 5: The RF Helicon-based Plasma Thruster (Render) [3].

The injector is movable along the symmetry axis z. It is made of conductive material to fine-tune the thruster's resonance frequency. The solenoid is located externally to produce the static magnetic field up to $\vec{B}_0 = 70\,\mathrm{mT}$ at $I_{sol} = 15\,\mathrm{A}$, the upper limit is to ensure more than 30 min operation without external cooling. The birdcage antenna is in a high pass configuration with 8 legs designed to resonate at $f = 40.68\,\mathrm{MHz}$. It is fed at one point, providing linear polarization of the EM fields. The commercial 3D EM software Remcom Inc. XFdtd® 7.8.1.3 is used to compute the propagation of the waves generated by the antenna, and obtain the resonance spectrum of the thruster to support the design, especially the choice of the correct capacitance. The thruster structure is of brass to 1) minimize Eddie currents due to the RF fields, 2) minimize interactions with $\vec{B}_0$. The birdcage antenna is enclosed within a brass Faraday shield that isolates the outer environment from the EM fields created by the antenna and vice versa, finally creating a resonant cavity. The simulations performed with XFdtd® show the frequency dependence of S_{11} (scattering parameter), and of Z, see Fig. 6 and Fig. 7. At each peak of S_{11} corresponds $X = 0\,\Omega$, being a resonant frequency. To verify that the correct mode $k = 1$ is achieved, the EM fields are visualized in 3D over time, verified to be linearly polarized and compared to the other peaks, see Fig. 8. At each wave cycle the EM fields reverse their directions. Once the correct resonance peak is identified, the capacitance value is varied until the corresponding $k = 1$ peak is at $40.68\,\mathrm{MHz}$. The required capacitance is finally $C = 785.51\,\mathrm{pF}$ per each gap.

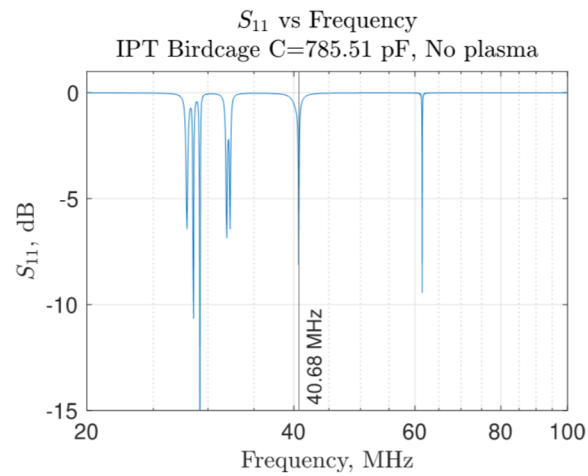

Figure 6: S_{11} vs f [3].

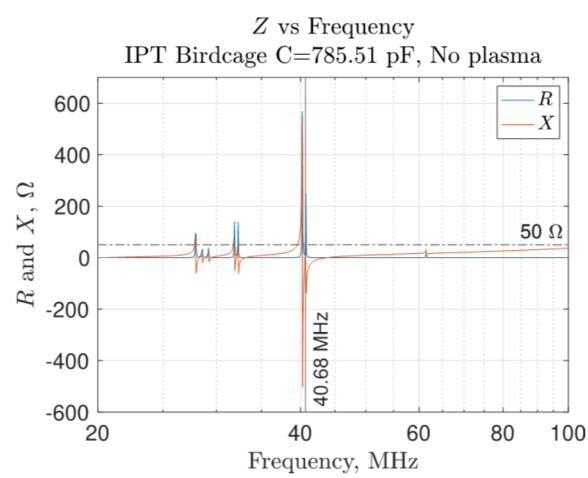

Figure 7: Z vs f [3].

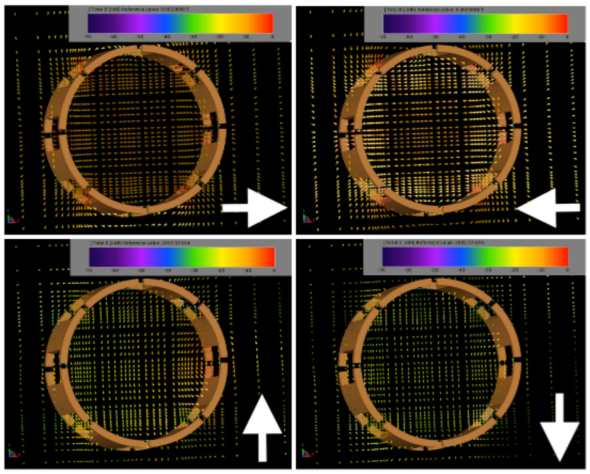

Figure 8: $\vec{B}_1$ (top) and $\vec{E}_1$ bottom over time [3].

6 RESONANCE TUNING

Deviations from the desired resonance frequency and impedance arise due to tolerances in manufacturing, assembly, and non-ideal electrical components, such as the capacitors. While further tuning is achieved during the birdcage antenna integration phase, the fine-tuning is a built-in mechanism in the thruster by shifting the conductive injector along the z axis. Once the thruster is fully assembled and integrated onto the vacuum chamber, the injector is used to fine-tune the resonance frequency. The assembled thruster is shown in Fig. 5.

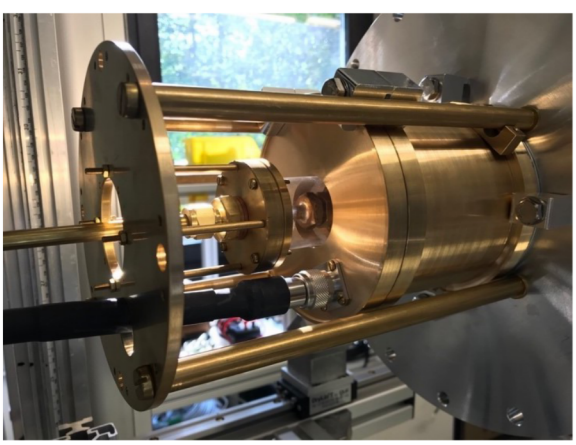

Figure 9: RF Helicon-based Plasma Thruster [3].

7 TESTING

B-field

The assembled thruster is connected to NanoVNA v2 network analyser to measure S_{11} and impedance Z that is calibrated beforehand. Such device operates in the range of $50\,\text{kHz} - 3\,\text{GHz}$, with a resolution of $10\,\text{kHz}$, a S_{11} noise floor of $-50\,\text{dB}$ and a system dynamic range of $70\,\text{dB}$ for $f < 1.5\,\text{GHz}$. The performance after final tuning is shown in Fig. 10, resulting in an $S_{11} = -47.3\,\text{dB}$ and $Z = (50.18 + 0.39\text{i})\,\Omega$ corresponding in $> 99.9\%$ of the power coupled in the antenna.

E-field

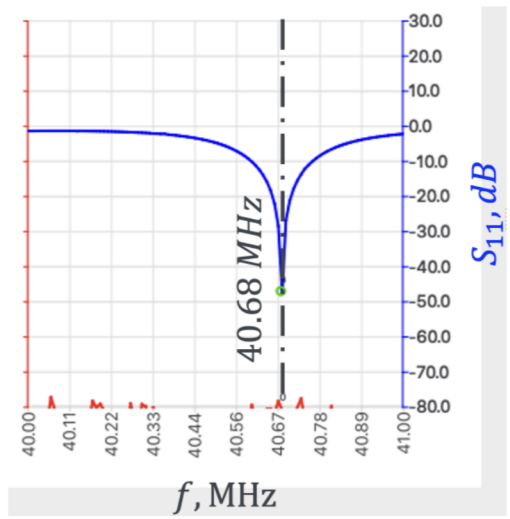

Figure 10: RF Helicon-based Plasma Thruster Measured Electrical Performance.

The first discharge characterization campaign of the thruster has been recently completed. Data are still being analysed, therefore, three exemplary conditions are shown. The thruster operating on Ar, N_2, and O_2, is shown in Fig. 11, Fig. 12, and Fig. 13 respectively. The images are taken through a quartz window with the same camera exposure settings. The test input parameters are a forward power $P_f = 60\,\text{W}$, solenoid current $I_S = 6.7\,\text{A}$ corresponding to $\vec{B}_0 \sim 30 - 40\,\text{mT}$, a particle flux equal for the three conditions of $\dot{N} = 20.30\,1/\text{s}^{-1}$, and a background pressure of $p_{ch} = 0.12 - 0.23\,\text{Pa}$. A further reduction of reflected power P_r is observed by tuning $\vec{B}_0$.

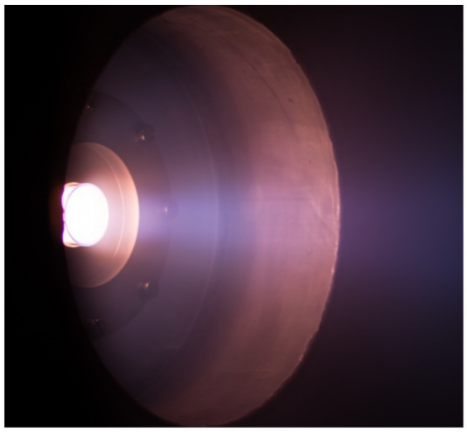

Figure 11: RF Helicon-based Plasma Thruster Operating on Argon [15].

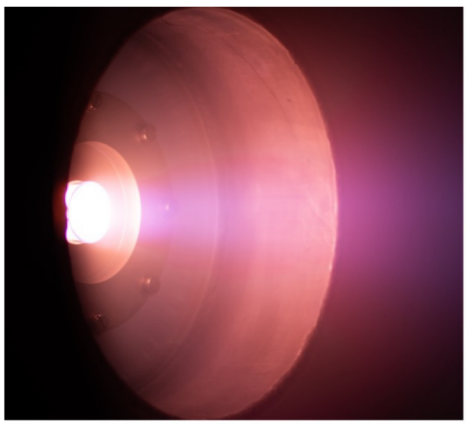

Figure 12: RF Helicon-based Plasma Thruster Operating on Nitrogen [15].

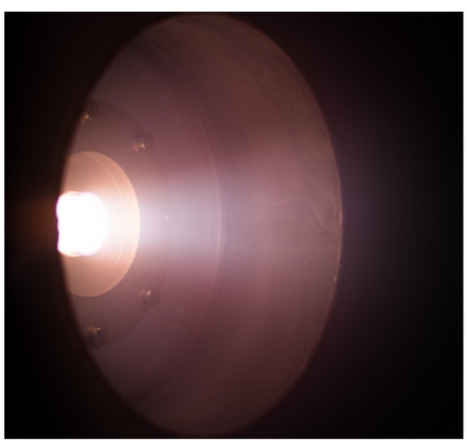

Figure 13: RF Helicon-based Plasma Thruster Operating on Oxygen [15].

8 MAGNETIC INDUCTIVE B-DOT PROBE

Finally, a 3-axis magnetic inductive B-dot probe has been designed and built with the aim of detecting the rotating magnetic field of the helicon waves in the plasma plume [14, 16, 17]. The probe is made of three small $N = 5$ turns coils with $\phi = 0.2\,\mathrm{mm}$ wire, and a coil area respectively of $A_x = 16\,\mathrm{mm}^2$, $A_y = 25\,\mathrm{mm}^2$, and $A_z = 36\,\mathrm{mm}^2$, that detect time-varying magnetic fields as they induce a voltage V on the coils with an angular frequency $\omega = 2\pi f$, see Eq. 4.

$$V = -NA\left|\frac{dB_{tot}}{dt}\right| = -NA\omega|B| \tag{4}$$

The material of the probe is mainly PEEK due to mechanical strength and relatively high melting temperature, an additional cover made of quartz is added to protect the probe from the direct plasma bombardment. The measured signal of each coil ends into one single RF power combiner (one per axis) to remove the capacitive pick-up that arises between plasma and coils, see Fig. 14. The probe has been integrated and is undergoing first calibrations.

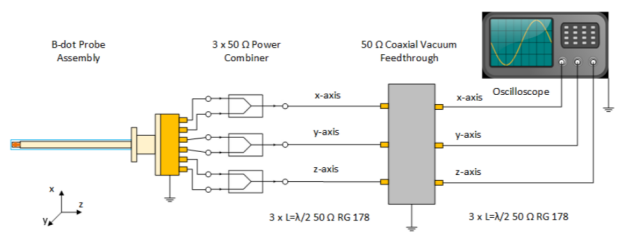

Figure 14: Magnetic Inductive B-dot Probe.

9 CONCLUSION

The RF Helicon-based plasma thruster based on a cylindrical birdcage antenna has been designed, the antenna electrical properties verified, ignited, and tested. It has the advantage of being optimized from the electrical point of view by providing a matched load, therefore minimizing power losses in terms of reflection and antenna heating. Moreover, the resulting EM fields generated are in an optimal configuration for accelerating a quasi-neutral plasma. The presence of an external static magnetic field is one of the boundary condition required for the formation of helicon waves within the

plasma, as well as providing the diverging magnetic field at the exhaust section to further produce thrust. The first test campaign has shown efficient power coupling at low power, minimized reflected power that can be further tuned by the applied magnetic field, and operated on multiple propellants based on ABEP with unchanged requirements. Furthermore, a magnetic inductive 3-axes B-dot probe has been designed and built and is undergoing calibration with the final aim of verifying the presence of helicon waves within the plasma plume. Further work is the testing with the B-dot probe followed by electrostatic probe measurements such as Langmuir, Faraday, and Retarding Potential Analyzer.

10 ACKNOWLEDGEMENTS

This project has received funding from the European Union's Horizon 2020 research and innovation programme under grant agreement No. 737183. This reflects only the author's view and the European Commission is not responsible for any use that may be made of the information it contains.

References

[1] Roberts, P., Crisp, N., Abrao Oiko, V., Edmondson, S., Haigh, S., Huyton, C., Livadiotti, S., Lyons, R., Smith, K., Sinpetru, L., Straker, A., Worrall, S., Romano, F., Herdrich, G., Boxberger, A., Chan, Y.A., Traub, C., Fasoulas, S., Smith, K., Outlaw, R., Becedas, J., Domínguez, R., González, D., Hanessian, V., Mølgaard, A., Nielsen, J., Bisgaard, M., Garcia-Almiñana, D., Rodriguez-Donaire, S., Sureda, M., Kataria, D., Villain, R., Perez, J.S., Conte, A., Belkouchi, B., Schwalber, A. & Heißerer, B. (October 2019). DISCOVERER – Making Commercial Satellite Operations in Very Low Earth Orbit a Reality, *70th International Astronautical Congress, Washington D.C., USA*, (IAC-19.C2.6.1x50774).

[2] Hayes, C.E., Edelstein, W.A., Schenck, J.F., Mueller, O.M. & Eash, M. (1985). An efficient, highly homogeneous radiofrequency coil for whole-body NMR imaging at 1.5 T, *Journal of Magnetic Resonance (1969)*, **63**(3), 622 – 628, ISSN 0022-2364, doi:https://doi.org/10.1016/0022-2364(85)90257-4.

[3] Romano, F., Chan, Y.A., Herdrich, G., Traub, C., Fasoulas, S., Roberts, P., Smith, K., Edmondson, S., Haigh, S., Crisp, N., Oiko, V., Worrall, S., Livadiotti, S., Huyton, C., Sinpetru, L., Straker, A., Becedas, J., Domínguez, R., González, D., Cañas, V., Sulliotti-Linner, V., Hanessian, V., Mølgaard, A., Nielsen, J., Bisgaard, M., Garcia-Almiñana, D., Rodriguez-Donaire, S., Sureda, M., Kataria, D., Outlaw, R., Villain, R., Perez, J., Conte, A., Belkouchi, B., Schwalber, A. & Heißerer, B. (2020). RF Helicon-based Inductive Plasma Thruster (IPT) Design for an Atmosphere-Breathing Electric Propulsion system (ABEP), *Acta Astronautica*, **176**, 476 – 483, ISSN 0094-5765, doi:https://doi.org/10.1016/j.actaastro.2020.07.008.

[4] Cifali, G., Misuri, T., Rossetti, P., Andrenucci, M., Valentian, D., Feili, D. & Lotz, B. (September 2011). Experimental characterization of HET and RIT with atmospheric propellants, *32nd International Electric Propulsion Conference, Wiesbaden, Germany*, (IEPC 2011 224).

[5] Cifali, G., Dignani, D., Misuri, T., Rossetti, P., Andrenucci, M., Valentian, D., Marchandise, F., Feili, D. & Lotz, B. (May 2012). Completion of HET and RIT characterization with atmospheric propellants, *Space Propulsion 2012, Bordeaux, France*, (SP2012 2355386).

[6] Cifali, G., Andrenussi, T., Giannetti, V., Leoprini, A., Rossodivita, A., Andrenucci, M., Barral, S., Longo, J. & Walpot, L. (May 2016). Experimental validation of a RAM-EP concept based on Hall-effect thruster, *Space Propulsion 2016, Rome, Italy*, (SP2016 3125202).

[7] Masillo, S., Romano, F., Soglia, R., Herdrich, G., Roberts, P., Boxberger, A., Chan, Y.A., Traub, C., Fasoulas, S., Smith, K., Edmondson, S., Haigh, S., Crisp, N., Oiko, V.A., Lyons, R., Worrall, S., Livadiotti, S., Huyton, C., Sinpetru, L., Outlaw, R., Becedas, J., Domínguez, R., González, D., Hanessian, V., Mølgaard, A., Nielsen, J., Bisgaard, M., Garcia-Almiñana, D., Rodriguez-Donaire, S., Sureda, M., Kataria, D., Villain, R., Perez, J.S., Conte, A., Belkouchi,

B., Schwalber, A., Heißerer, B., Magarotto, M. & Pavarin., D. (October 2018). Analysis of electrodeless plasma source enhancement by an externally applied magnetic field for an inductive plasma thruster (IPT), *7th Russian German Conference on Electric Propulsion and Their Application, Rauischholzhausen, Germany*, (RGCEP 2018 A079).

[8] Melazzi, D. & Lancellotti, V. (2014). ADAMANT: A surface and volume integral-equation solver for the analysis and design of helicon plasma sources, *Computer Physics Communications*, **185**(7), 1914 – 1925, ISSN 0010-4655, doi:https://doi.org/10.1016/j.cpc.2014.03.019.

[9] Kieckhafer, A.W. & Walker, M.L.R. (2010). RF power system for thrust measurements of a helicon plasma source, *Review of Scientific Instruments*, **81**(7), 075106, doi:10.1063/1.3460263.

[10] Guittienne, P., Howling, A. & Hollenstein, C. (2014). Analysis of resonant planar dissipative network antennas for RF inductively coupled plasma sources, *Plasma Sources Science and Technology*, **23**(1), 015006.

[11] Howling, A., Guittienne, P., Hollenstein, C. & Furno, I. (2014). Resonant RF network antennas for inductively-coupled plasma sources, *Proceeding 41st EPS Conference on Plasma Physics, Berlin, Germany, 23-27 June 2014*, CONF, pp. P2–139.

[12] Furno, I., Agnello, R., Duval, B., Marini, C., Howling, A., Jacquier, R., Guittienne, P., Usel, F., Dirk, W., Alain, S. & Stephane, B. (2016). A novel helicon plasma source for negative ion beams for fusion, URL `http://infoscience.epfl.ch/record/222962`.

[13] Furno, I., Agnello, R., Fantz, U., Howling, A., Jacquier, R., Marini, C., Plyushchev, G., Guittienne, P. & Simonin, A. (2017). Helicon wave-generated plasmas for negative ion beams for fusion, *EPJ Web of Conferences*, volume 157, p. 03014, EDP Sciences.

[14] Jacquier, R., Agnello, R., Duteil, B.P., Guittienne, P., Howling, A., Plyushchev, G., Marini, C., Simonin, A., Morgal, I., Bechu, S. et al. (2019). First B-dot measurements in the RAID device, an alternative negative ion source for DEMO neutral beams, *Fusion Engineering and Design*, ISSN 0920-3796, doi:https://doi.org/10.1016/j.fusengdes.2019.02.025.

[15] Romano, F., Herdrich, G., , Chan, Y.A. & et Al. (October 2020). RF Helicon-based Plasma Thruster (IPT): Design, Set-up, and First Ignition, *71st International Astronautical Congress, Online, The CyberSpace Edition*, (IAC-20,C4,5,11,x58032).

[16] Polzin, K.A., Hill, C.S., Turchi, P.J., Burton, R.L., Messer, S., Lovberg, R.H. & Hallock, A.K. (2017). Recommended practice for use of inductive magnetic field probes in electric propulsion testing, *Journal of Propulsion and Power*, **33**(3), 659–667.

[17] Bose, S., Kaur, M., Barada, K.K., Ghosh, J., Chattopadhyay, P.K. & Pal, R. (2018). Understanding the working of a B-dot probe, *European Journal of Physics*, **40**(1), 015803.